Fractal-driven universality in quantum transport through mesoscopic devices

F. M. Oliveira,[1,2] Louis G. C. S. Sá,[1] and J. G. G. S. Ramos[1]

[1]*Departamento de Física, Universidade Federal da Paraíba, 58051-970 João Pessoa, Paraíba, Brazil*
[2]*Chair of Adaptive Dynamic Systems, Technische Universität Dresden, 01062 Dresden, Germany*

(Received 12 July 2025; revised 10 March 2026; accepted 28 May 2026; published 15 June 2026)

We examine the impact of spatial fractality on universal quantum transport in mesoscopic systems featuring Sierpiński carpet scattering geometries. Transport calculations are performed using the nonequilibrium Green's function formalism within the Landauer-Büttiker framework, allowing for a detailed statistical characterization of conductance and shot noise power fluctuations. Our analysis reveals that the fractal dimension of these fluctuations increases systematically with the iteration depth of the structure, reflecting enhanced complexity in quantum interference patterns. A direct and robust correlation is established between the Hausdorff dimension of the scattering region and the effective fractal dimension of transport observables, independent of the Wigner-Dyson universal symmetry class (GOE, GUE, and GSE). This provides compelling evidence that scattering across internal lacunae constitutes the dominant mechanism shaping transport behavior in the universal regime. Moreover, we find that the density of local extrema increases while the correlation length decreases with increasing fractality; however, the number of extrema per correlation length remains remarkably with negligible variation. Notably, the autocorrelation functions progressively deviate from the standard Lorentzian form, indicating that geometric self-similarity introduces nontrivial modifications to the spectral correlations predicted by Random Matrix Theory.

DOI: 10.1103/h6yp-4fty

I. INTRODUCTION

The statistical behavior of open quantum systems has emerged as a central theme in modern theoretical and experimental physics [1–3]. The observation of irregular resonance spectra in nuclear scattering processes [4,5] historically motivated Wigner's pioneering hypothesis of modeling complex Hamiltonians using random matrices [6,7]. This conceptual framework later evolved into Random Matrix Theory (RMT), a cornerstone in the study of quantum chaos [8–11]. In contemporary devices, quantum chaotic scattering is now probed with remarkable precision via engineered mesoscopic systems, notably quantum dots, which offer controlled devices for investigating coherent transport phenomena [12–14].

Quantum interference effects in coherent transport through quantum dots manifest in a range of observable signatures [15–18], among which universal conductance fluctuations (UCFs) are particularly prominent [13,19]. These fluctuations, arising from multiple scattering paths within the dot, exhibit sample-specific yet reproducible variations in conductance as external control parameters such as the Fermi energy ε or magnetic field B are continuously tuned [20,21]. Crucially, the statistical features of UCFs are determined not by the microscopic details of the device but by its global symmetry class, as established in the Wigner-Dyson classification [22], encompassing the orthogonal ($\beta = 1$), unitary ($\beta = 2$), and symplectic ($\beta = 4$) ensembles [12].

Within the Landauer-Büttiker formalism [23,24], RMT successfully accounts for the amplitude and structure of the conductance correlation function (CF), which characterizes the statistical memory of the system under perturbations. For energy-dependent UCFs, the CF typically follows a Lorentzian profile, $C(\delta\varepsilon) \propto (1 + \delta\varepsilon^2)^{-1}$ [25,26], while in magnetoconductance fluctuations the decay adopts a squared-Lorentzian form, $C(\delta B) \propto (1 + \delta B^2)^{-2}$ [12,27]. These functional forms are not merely theoretical predictions—they impose measurable constraints on quantities such as the average density of extrema in conductance traces, which serve as practical indicators of underlying quantum chaos and spectral rigidity.

This observation naturally leads to a fundamental question: can a controllable physical parameter induce significant and measurable deviations from the universal forms of the correlation function predicted by RMT? This investigation examines the role of spatial geometry, focusing on fractal structures [28–30] engineered at the nanoscale within quantum dot systems, to assess their influence on quantum transport propertieson of such structures within quantum dot architectures. We demonstrate that the shape of the conductance correlation function can be systematically modulated by altering the fractal characteristics of the scattering region, thus enabling deliberate departures from the canonical universal profiles. Our findings reveal a geometric influence: remarkably, the same set of statistical signatures emerges in both the spatial and spectral (energy-dependent) domains of the quantum transport regime, suggesting a deep correspondence between the morphology of the system and the topology of its universal fluctuation landscape.

The advent of fractal geometry, originally formalized by Benoît Mandelbrot, has provided an essential mathematical framework for describing complex systems exhibiting scale invariance and noninteger (fractal) dimensionality—features that are pervasive in both natural and artificial structures.

The confluence of mesoscopic transport and fractal architectures has recently attracted growing attention, offering a novel platform to explore quantum interference in non-Euclidean landscapes [31–33]. Experimental and theoretical investigations involving deterministic fractal configurations, such as Sierpiński triangles, gaskets, and carpets, have shown that these structures can serve as effective quantum corrals, confining wavefunctions in spatially elaborate environments and thereby enriching the interference landscape [34–38].

Although prior studies have qualitatively linked the fractal dimension of the scattering region to enhancements in signal complexity [39–41], a quantitative exploration of how fractality governs UCFs —including metrics such as the density of extrema, the decay of the correlation function, and shot noise statistics—remains underdeveloped. In this work we address this gap by providing a comprehensive analysis of quantum transport in Sierpiński carpet geometries, elucidating how fractal iteration directly imprints itself on the statistical fabric of observables in the universal regime.

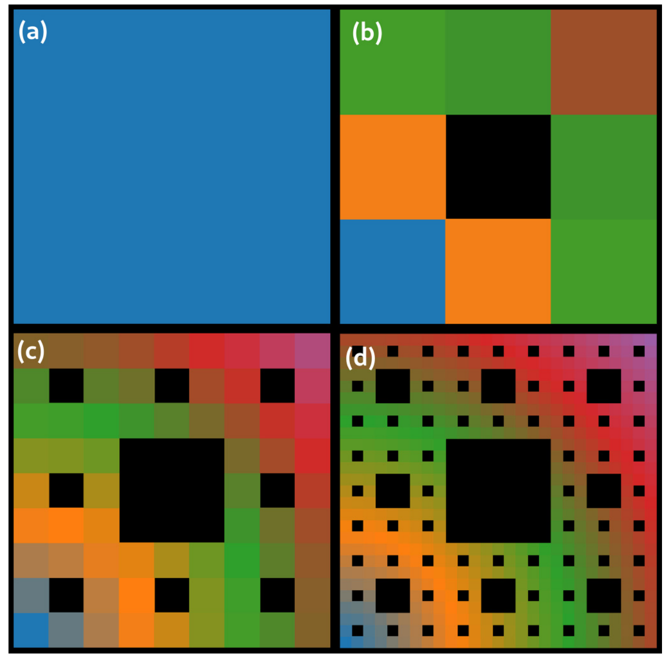

FIG. 1. Artistic representation of the Sierpiński carpet at different recursion levels: (a) $m = 0$, (b) $m = 1$, (c) $m = 2$, and (d) $m = 3$. At each iteration step, the central square of side length $(L/3)^m$ is recursively removed from every remaining subregion, generating the self-similar fractal structure.

II. THEORETICAL AND COMPUTATIONAL FRAMEWORK

In this investigation we study quantum transport properties in mesoscopic systems. To this end we employ a formalism based on the nonequilibrium Green's function (NEGF) approach within the Landauer-Büttiker framework, which provides a rigorous and general method for computing transmission and noise properties in phase-coherent conductors [42–46]. The numerical implementation of this formalism is carried out using the KWANT software package, a Python-based toolkit for quantum transport simulations in tight-binding models [47].

In this approach, the system is modeled as a finite scattering region connected to semi-infinite leads. The central quantity for transport analysis is the retarded Green's function $G^r(E)$, defined as

$$G^r(E) = [E + i\eta - H - \Sigma_L(E) - \Sigma_R(E)]^{-1}, \tag{1}$$

where E is the Fermi energy, η is a positive infinitesimal, H is the Hamiltonian of the central region, and $\Sigma_{L,R}(E)$ are the self-energy terms due to the left and right leads, respectively. These self-energies encapsulate the effect of the infinite leads on the finite system and are computed analytically for ideal leads or numerically when necessary.

The transmission coefficient $T(E)$ is obtained from the Caroli formula,

$$T(E) = \mathrm{Tr}[\Gamma_L(E)G^r(E)\Gamma_R(E)G^a(E)], \tag{2}$$

where $G^a(E) = [G^r(E)]^\dagger$ is the advanced Green's function, and $\Gamma_{L,R}(E) = i[\Sigma_{L,R}(E) - \Sigma^\dagger_{L,R}(E)]$ are the broadening matrices associated with the leads. The dimensionless conductance (in units of e^2/h) is then directly given by $G(E) = T(E)$ at zero temperature.

Shot noise power, arising from the granularity of charge and quantum partitioning at the interfaces, is characterized by the noise power $P(E)$ [48–50]. Under zero-temperature conditions, the shot noise power is related to the transmission matrix via [51,52]

$$P(E) = T(E)[1 - T(E)], \tag{3}$$

in units of $2e^3V/h$, where V is the applied bias. For multichannel systems, the full transmission matrix t is considered, and the shot-noise power generalizes to

$$\mathcal{P}(E) = \mathrm{Tr}[t^\dagger(E)t(E)(\mathbb{I} - t^\dagger(E)t(E))]. \tag{4}$$

The system parameters and geometries are carefully tuned to explore the interplay between quantum interference, disorder, and classical chaos. To implement fractal geometries within a quantum transport framework, we construct atomistic tight-binding lattices using the KWANT package. Specifically, we begin with a regular square lattice, which serves as a discretized representation of a two-dimensional electron gas (2DEG) under coherent transport conditions. Fractal properties are introduced by selectively removing lattice sites in accordance with the recursive rules defining the Sierpiński carpet. This approach allows for the realization of deterministic fractal structures at the atomic level, effectively embedding spatial self-similarity into the tight-binding Hamiltonian. As such, the quantum system inherits the geometric complexity of the underlying lattice, enabling the investigation of how fractality influences electronic transport and related observables.

The Sierpiński carpet depicted in Fig. 1 is a paradigmatic example of a deterministic fractal. Its construction is recursive and begins with a square of linear size L. At the first iteration ($m = 1$), a square of side length $L/3$ is removed from the center of the original square, resulting in a structure composed of eight remaining subsquares [28,29].

This construction process can be repeated indefinitely. At each step, the same removal operation is applied to all remaining squares from the previous iteration, with the central portion of each being excised at a reduced scale. Specifically, at step $m = 2$, the operation is applied to each of the eight subsquares of side $L/3$, removing central squares of side $L/9$, yielding a total of 8^2 surviving subsquares. Thus, the procedure generates a self-similar structure composed of 8^m squares of side length $(L/3)^m$ at recursion level m.

Formally, the number of surviving subregions at iteration m is given by

$$N_m = 8^m, \tag{5}$$

as each recursive step subdivides every square into nine equal parts and retains eight of them. The area of each retained square at step m is

$$a_m = \left(\frac{1}{3}\right)^{2m} L^2, \tag{6}$$

so the total area at recursion level m is

$$A_m = N_m a_m = \left(\frac{8}{9}\right)^m L^2. \tag{7}$$

As $m \to \infty$, it follows that $A_m \to 0$, i.e., the total area of the structure vanishes in the limit, while the geometric boundary remains nontrivial. This property underlies the fractal nature of the Sierpiński carpet: it is a closed structure with a nonzero perimeter and zero Lebesgue measure in the limit.

From the standpoint of similarity dimension, the fractal dimension d of a self-similar object can be defined through the scaling relation

$$M(\theta L) = \theta^d M(L), \tag{8}$$

where $M(L)$ denotes the number of self-similar components at scale L, and $\theta < 1$ is the linear scaling factor. For the Sierpiński carpet at $m = 1$ and $L = 1$, we have $M(L) = 8$, since the figure consists of eight squares of side length $1/3$. Therefore, $\theta = 1/3$, and at the previous step ($m = 0$), we had $M(\theta L) = 1$.

Substituting into Eq. (8), we obtain

$$d = \frac{\ln(1/8)}{\ln(1/3)} = \frac{-\ln(8)}{-\ln(3)} = \frac{\ln(8)}{\ln(3)} \approx 1.8928\ldots. \tag{9}$$

This exponent d corresponds to the Hausdorff (or similarity) dimension of the fractal. It provides an exact analytical measure of the geometric complexity of the Sierpiński carpet and characterizes how its structure occupies space at different length scales. Numerical estimations of the fractal dimension for increasingly large recursion depths m converge to this analytical value, offering a benchmark for computational consistency and precision in the analysis of self-similar quantum systems.

III. STATISTICAL SIGNATURES OF THE UNIVERSAL MESOSCOPIC REGIME: CONDUCTANCE AND SHOT-NOISE POWER FLUCTUATIONS

This section provides a systematic and quantitative investigation of quantum electronic transport properties, specifically the conductance (G) and shot noise power (P), in mesoscopic systems exhibiting Sierpinski carpet geometries as depicted in Fig. 1. The choice of this class of fractal structures is motivated by their capacity to exhibit nontrivial topological features and complex self-similar spatial inhomogeneities, which profoundly affect the transport characteristics compared to both periodic and conventionally disordered Euclidean systems [53–55]. Numerical simulations were performed on scattering regions constructed at successive fractal iterations $m = 0, 1, 2, 3,$ and 4, where $m = 0$ corresponds to a fully filled square (i.e., the nonfractal reference system). As the generation level m increases, the structure acquires increasing topological complexity and decreasing effective connectivity, accompanied by a reduction in the fractal dimension d_f. This progression inherently introduces a geometrically induced disorder that complements the externally imposed Anderson-type disorder. Such geometric complexity gives rise to anomalous transport phenomena, the analysis of which can shed light on the interplay between structural disorder and quantum coherence in non-Euclidean mesoscopic systems.

Signatures of Quantum Chaos in UCFs

To rigorously characterize the UCF regime in mesoscopic systems with fractal geometries, we performed detailed numerical simulations on Sierpiński carpet structures at various iteration levels $m = 0$ to 4.

In this work we investigate electronic transport through chaotic semiconductor quantum dots belonging to the three universal Wigner-Dyson symmetry classes $\beta \in \{1, 2, 4\}$, corresponding respectively to the orthogonal, unitary, and symplectic ensembles of random matrix theory. These symmetry classes arise from the presence or absence of time-reversal and spin-rotation symmetries and determine the universal statistical properties of mesoscopic transport, including UCFs.

To model a confined 2DEG we employ a tight-binding discretization of the effective mass Hamiltonian on a square lattice. Within this framework the different symmetry classes can be implemented by progressively breaking the relevant symmetries through magnetic fields and spin-orbit interactions.

The Hamiltonian describing the orthogonal class ($\beta = 1$) reads

$$H_1 = \sum_{i,\sigma} \varepsilon_i c_{i\sigma}^\dagger c_{i\sigma} - t \sum_{\langle i,j\rangle,\sigma} c_{i\sigma}^\dagger c_{j\sigma}, \tag{10}$$

where $c_{i\sigma}^\dagger$ ($c_{i\sigma}$) creates (annihilates) an electron with spin σ at lattice site i. The hopping amplitude t is related to the effective mass approximation of the 2DEG and the on-site energies ε_i represent short-range disorder, randomly distributed within

$$-W/2 < \varepsilon_i < W/2,$$

where W quantifies the disorder strength.

Time-reversal symmetry can be broken by applying a perpendicular magnetic field B, introduced through the Peierls substitution in the hopping amplitudes. The Hamiltonian of the unitary class ($\beta = 2$) is therefore written as

$$H_2 = \sum_{i,\sigma} \varepsilon_i c_{i\sigma}^\dagger c_{i\sigma} - t \sum_{\langle i,j\rangle,\sigma} e^{i\phi_{ij}} c_{i\sigma}^\dagger c_{j\sigma}, \tag{11}$$

where the Peierls phase factor is

$$\phi_{ij} = \frac{e}{\hbar} \int_{\mathbf{r}_i}^{\mathbf{r}_j} \mathbf{A} \cdot d\mathbf{l}, \tag{12}$$

with $\mathbf{A}$ being the vector potential associated with the magnetic field. For a perpendicular field we adopt the Landau gauge $\mathbf{A} = (-By, 0, 0)$.

Finally, the symplectic class ($\beta = 4$) is obtained by introducing spin-orbit interaction, which breaks spin-rotation symmetry while preserving time-reversal symmetry. In the presence of Rashba spin-orbit coupling the Hamiltonian becomes

$$H_3 = H_1 + i\lambda_R \sum_{\langle i,j\rangle} c_i^\dagger (\mathbf{s} \times \hat{\mathbf{d}}_{ij})_z c_j, \tag{13}$$

where $\mathbf{s} = (s_x, s_y, s_z)$ are the Pauli matrices acting on the spin degree of freedom, $\hat{\mathbf{d}}_{ij}$ is the unit vector connecting neighboring lattice sites, and λ_R denotes the Rashba coupling strength.

Within this framework the three Hamiltonians realize the universal Wigner-Dyson symmetry classes: H_1 preserves both time-reversal and spin-rotation symmetries (orthogonal ensemble), H_2 breaks time-reversal symmetry through the magnetic field (unitary ensemble), and H_3 breaks spin-rotation symmetry via spin-orbit interaction while maintaining time-reversal symmetry (symplectic ensemble).

In the numerical implementation, these Hamiltonians are substituted into Eq. (1) in order to compute the scattering matrix of the open quantum dot. From the resulting scattering matrix we extract the transmission block t, which is then employed in the Landauer-Büttiker formulation to evaluate the conductance as well as the shot-noise power defined in the previous section.

Disorder was introduced by adding a stochastic perturbation to the local potential, with the disorder strength W varied from 0 to 4 in increments. For each W, 5000 independent disorder realizations were generated to ensure statistical reliability.

The ensemble-averaged conductance per channel and its root-mean-square fluctuation rms(G) were computed for each configuration. As shown in Fig. 2, $\langle G\rangle$ per total open channels N decreases monotonically with increasing disorder strength W, reflecting enhanced electron scattering and the progressive onset of localization effects. The value of W at which rms(G) attains its peak corresponds to the UCF regime, characterized by conductance fluctuations of order e^2/h, independent of system-specific details [22,56]. In the diffusive regime considered here, the ensemble-averaged conductance per channel remains nonuniversal, whereas the root-mean-square fluctuation rms(G) converges to the UCF value, which is the primary focus of this work. For completeness, the corresponding universal values of rms(G) for the three Wigner-Dyson symmetry classes, expressed in units of e^2/h, are $\sqrt{8/15}\, e^2/h \approx 0.730\, e^2/h$ for the orthogonal class ($\beta = 1$), $\sqrt{4/15}\, e^2/h \approx 0.516\, e^2/h$ for the unitary class ($\beta = 2$), and $\sqrt{2/15}\, e^2/h \approx 0.365\, e^2/h$ for the symplectic class ($\beta = 4$).

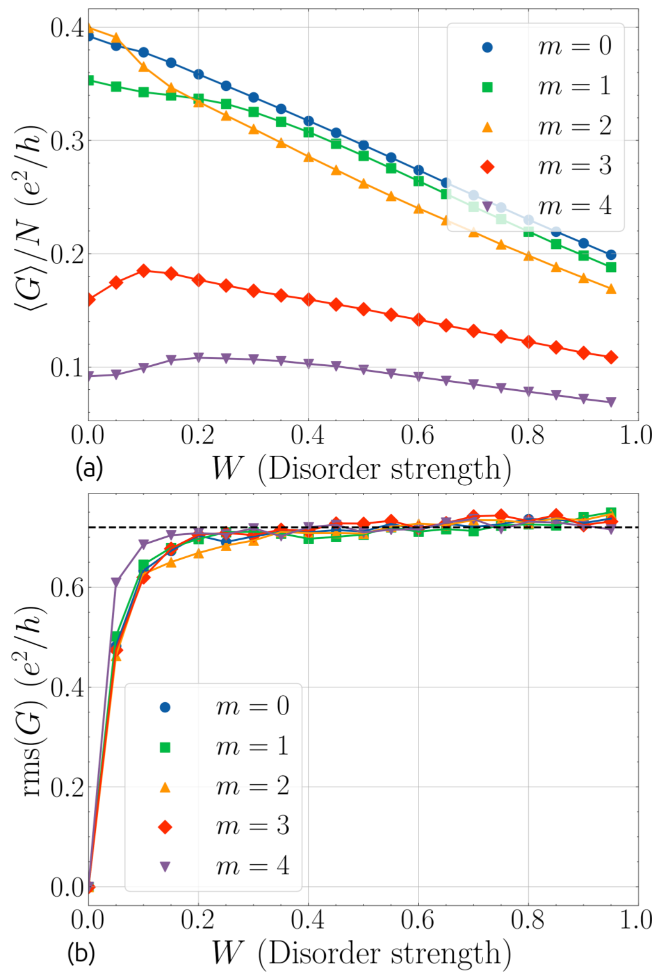

FIG. 2. (a) Ensemble-averaged conductance $\langle G\rangle$ per total open channels N as a function of the disorder strength W for Sierpinski carpets at different iteration levels m. (b) Root-mean-square conductance fluctuation rms(G) as a function of the disorder strength W for the same systems. Results are shown for $\beta = 1$ and a system containing $N = 88\,209$ lattice sites.

Remarkably, even in the absence of potential disorder ($W = 0$), $\langle G\rangle$ decreases systematically with increasing fractal iteration level m. This behavior indicates that the geometric complexity of the fractal structure itself acts as a source of effective structural disorder, which can be interpreted as a reduction in the number of resonant states available near the Fermi energy.

The values of W corresponding to the UCF regime for each iteration level are $W_{m=0} = 0.797$, $W_{m=1} = 0.646$, $W_{m=2} = 0.551$, $W_{m=3} = 0.391$, and $W_{m=4} = 0.291$.

Subsequent analyses involved computing the conductance and shot noise power spectrum as functions of the Fermi energy within the universal regime for each m, as depicted in Figs. 2 and 3. These computations were conducted under the framework of the three canonical RMT ensembles. The results are consistent with the predictions of RMT, confirming the universality of conductance fluctuations in these fractal systems. The root-mean-square (rms) values of the conductance fluctuations converge to the characteristic values of the Wigner-Dyson ensembles.

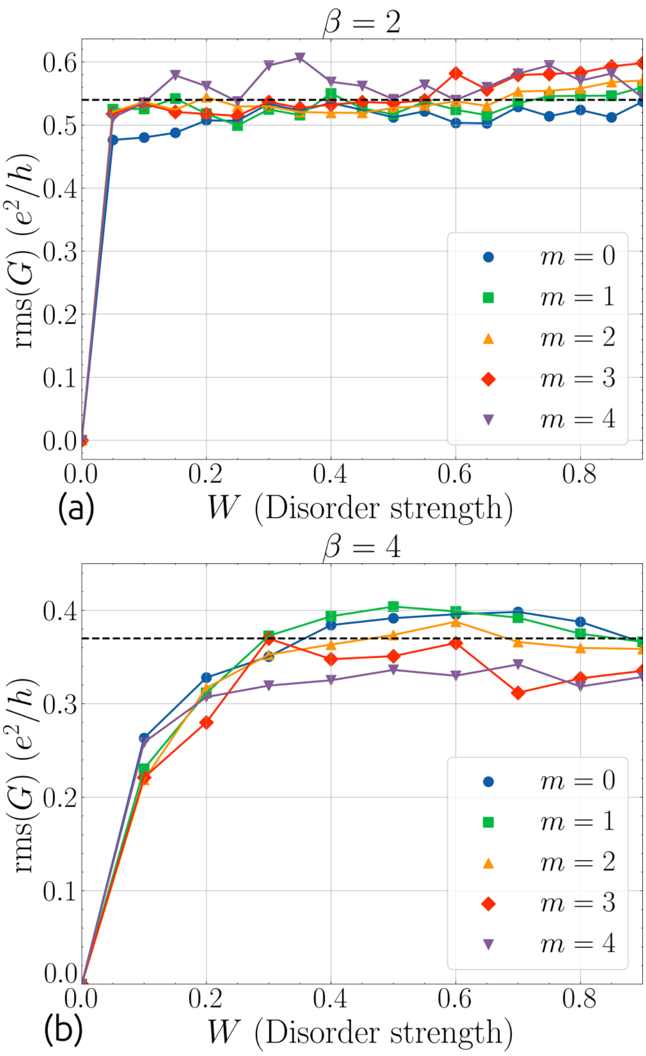

FIG. 3. (a) The universal regime is reached for the ensembles with $\beta = 2$ and $\beta = 4$. (b) Root-mean-square conductance fluctuation rms(G) as a function of the disorder strength W for Sierpinski carpet structures at different iteration levels m. Results were obtained for a system containing $N = 88\,209$ lattice sites.

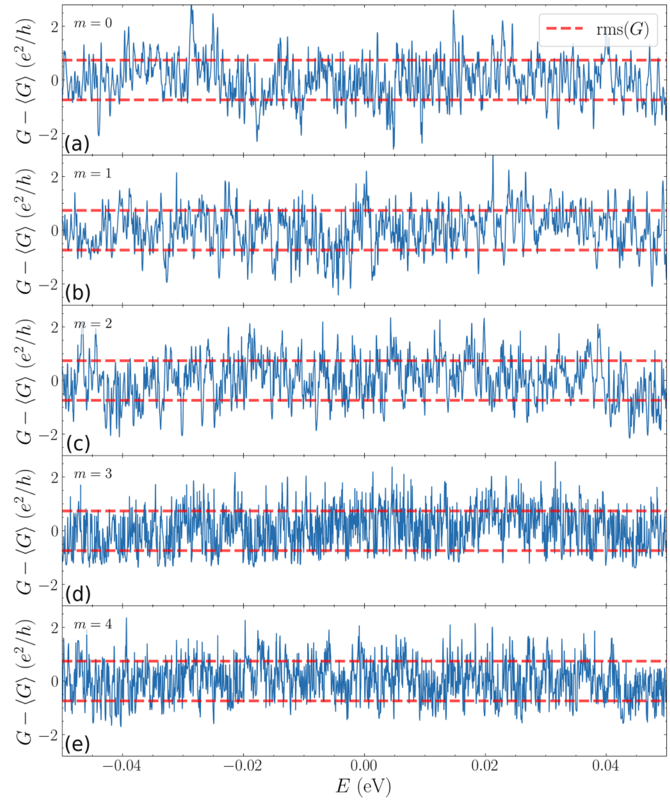

FIG. 4. Representative conductance fluctuation signals, $G - \langle G\rangle$, as a function of energy for the $\beta = 1$ ensemble. Panels (a) through (e) correspond to fractal iteration levels $m = 0$ to $m = 4$, respectively. An increase in iteration level leads to more intricate fluctuation patterns. The variance of the fluctuations remains approximately constant, with rms$(G) \approx 0.730\,e^2/h$ in all panels, as indicated by the horizontal dashed line. Results obtained for a system containing $N = 88\,209$ lattice sites.

IV. FRACTAL DIMENSIONS IN QUANTUM TRANSPORT: CONDUCTANCE AND SHOT NOISE IN SELF-SIMILAR SYSTEMS

The exploration of quantum transport phenomena in systems with intricate geometries has unveiled a profound interplay between structural complexity and electronic behavior. In particular, fractal geometries, such as the Sierpiński carpet, offer a fertile ground for investigating how self-similarity and noninteger dimensionality influence conductance and shot noise characteristics. This section presents a comprehensive analysis of the fractal dimensions of conductance and shot noise signals, employing the box-counting method to quantify their complexity across different fractal iteration levels.

The box-counting method, also known as the Minkowski-Bouligand dimension, is a widely adopted technique for estimating the fractal dimension of a set [28,29]. This method involves overlaying a grid of boxes of size ℓ over the graphical representation of the signal and counting the number of boxes $\mathcal{N}(\ell)$ that contain a part of the signal. By varying ℓ and analyzing how $\mathcal{N}(\ell)$ scales with ℓ, the fractal dimension D can be estimated using the relation

$$\mathcal{N}(\ell) \propto \ell^{-D}, \tag{14}$$

which, upon taking logarithms, yields

$$\log \mathcal{N}(\ell) = -D \log \ell + C, \tag{15}$$

where C is a constant. The fractal dimension D is thus obtained as the slope of the linear fit in a log-log plot of $\mathcal{N}(\ell)$ versus ℓ.

Figure 4 illustrates representative universal conductance signals as a function of energy for the $\beta = 1$ ensemble, corresponding to different fractal iteration levels $m = 0$ to $m = 4$. As the iteration level increases, the conductance curves exhibit increasingly complex fluctuations, indicative of enhanced structural intricacy in the underlying geometry.

The box-counting analysis was performed on these conductance and corresponding shot noise signals. Figure 5 presents the log-log plots of $\mathcal{N}(\ell)$ versus ℓ for these signals, along with the linear fits used to estimate the fractal dimensions. The linearity of these plots confirms the self-similar nature of the signals over the scales considered.

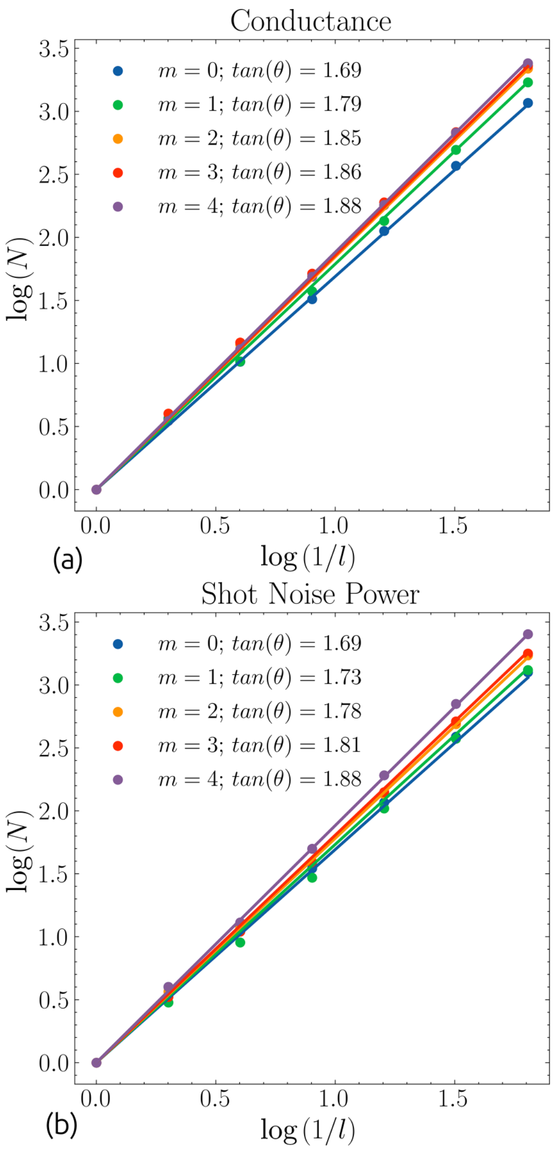

FIG. 5. (a) Log-log plots of the number of boxes $\mathcal{N}(\ell)$ versus box size ℓ for conductance signals and (b) shot noise signals in the $\beta = 1$ ensemble across fractal iteration levels $m = 0$ to $m = 4$. The slopes of the linear fits provide estimates of the fractal dimensions.

TABLE I. Estimated fractal dimensions for the conductance (G) and shot-noise (P) signals across different symmetry classes (β) and fractal iteration levels (m). In all cases, the estimated dimensions converge to the Hausdorff dimension of the Sierpiński carpet, $D \approx 1.89$, independently of the universal symmetry class and of the observable considered.

	$m = 0$	$m = 1$	$m = 2$	$m = 3$	$m = 4$
$\beta = 1$ (G)	1.69	1.79	1.85	1.86	1.88
$\beta = 2$ (G)	1.33	1.62	1.73	1.81	1.86
$\beta = 4$ (G)	1.19	1.44	1.75	1.80	1.86
$\beta = 1$ (P)	1.69	1.73	1.78	1.81	1.88
$\beta = 2$ (P)	1.45	1.67	1.73	1.65	1.85
$\beta = 4$ (P)	1.23	1.37	1.60	1.83	1.87

Table I summarizes the estimated fractal dimensions for conductance (G) and shot noise (P) signals across the three symmetry classes ($\beta = 1$, $\beta = 2$, and $\beta = 4$) and five fractal iteration levels. A clear trend emerges: the fractal dimension increases with the iteration level m, reflecting the growing complexity of the signals as the underlying geometry becomes more intricate.

The observed increase in fractal dimension with higher iteration levels signifies a transition towards more space-filling and complex signal patterns. This behavior aligns with the theoretical understanding that fractal geometries, such as the Sierpiński carpet with a Hausdorff dimension of approximately 1.89 [28,31,40,54,55,57,58], induce intricate electron pathways, leading to enhanced quantum interference effects and conductance fluctuations [29]. Moreover, the consistency of this trend across different symmetry classes suggests that the fractal-induced complexity in transport properties is a robust feature, largely independent of the specific symmetry considerations. This universality underscores the fundamental role of geometric complexity in shaping quantum transport phenomena.

The UCFs observed in mesoscopic systems with fractal geometries exhibit increasingly irregular and oscillatory behavior as the iteration step m of the fractal generation increases. This enhanced oscillatory structure across energy scales strongly suggests that the UCF traces possess fractal characteristics, with an effective dimension exceeding their topological dimension. To quantitatively analyze this behavior, we compute the fractal dimension of the UCFs using the box-counting (or Minkowski-Bouligand) method, a well-established approach for characterizing fractal sets.

Applying this methodology to the UCFs generated in our Sierpiński carpet systems, we find a well-defined linear scaling regime spanning more than two decades in ℓ, with the estimated fractal dimension consistently falling within the range $1 < D < 2$. This noninteger dimension confirms that the conductance traces are neither one-dimensional curves nor space-filling two-dimensional objects, but instead exhibit an intermediate, genuinely fractal morphology.

The emergence of fractality in the UCFs can be attributed to the complex interplay between localized and extended electronic states within narrow energy intervals. Notably, localized electronic wavefunctions arise in the presence of disorder-induced universal symmetries, even in the deterministic structure of the Sierpiński carpet. Crucially, our results indicate that electron scattering off the internal voids (lacunae) of the fractal structure constitutes the dominant mechanism modulating the physical observables in the universal regime. This effect supersedes any dependence on the microscopic configuration of impurities or the details of the interaction potential.

Furthermore, we have verified that the fractal dimension of the UCF traces remains invariant under changes in the positions of the leads, the fundamental symmetries of the system (e.g., time-reversal or spin-rotation symmetry), and the size of the scattering region. Such invariance strongly supports the conclusion that the observed fractality is an intrinsic geometrical property of the scattering landscape itself, and not an artifact of extrinsic parameters such as atomic composition or disorder profile.

This fractal analysis reveals that UCFs encode information about the geometry of the underlying structure at scales far below the mean-free path. Conversely, this finding implies that it is possible to engineer the fluctuation spectrum and correlation length of quantum transport by judiciously designing the geometry of the scattering region. The observation that the fractal dimension of the sample directly governs the fractal dimension of the conductance trace constitutes one of the central and most significant results of the present work.

The findings presented here open avenues for further exploration into the relationship between fractal geometry and quantum transport. Understanding these relationships not only enriches the theoretical framework of quantum transport in complex systems but also informs the design of novel materials and devices where control over electronic properties is achieved through geometric engineering.

V. STATISTICAL SIGNATURES OF THE UNIVERSAL MESOSCOPIC REGIME: AUTOCORRELATION AND PEAK DENSITY ANALYSIS

In addition to the fractality-induced effects discussed in the previous section, other physical phenomena reveal a direct relationship between fractal indices and observable quantities. One such observable is the density of local maxima in conductance and shot noise signals. We generated these signals for the random matrix ensembles $\beta = 1$, $\beta = 2$, and $\beta = 4$, across five distinct fractality levels considered in this study.

Figure 6 presents representative conductance traces for a typical realization within the $\beta = 1$ symmetry class. The simulations were carried out over a narrow energy window centered at $E = 0$, defined in units of the correlation length, Γ, of the Quantum Dots. A clear trend is observed: the density of local maxima systematically increases with the fractal iteration level m, indicating that the spatial complexity of the system exerts a direct influence on the frequency of extrema in the conductance fluctuations. Notably, we observe that the correlation length, Γ, decreases by approximately one order of magnitude when comparing the nonfractal case [$m = 0$, Fig. 6(a)] with the highly fractalized structure [$m = 4$, Fig. 6(e)]. In parallel, the density of maxima exhibits significantly more rapid fluctuations as m increases, suggesting a marked enhancement in spectral irregularity with fractal depth. Remarkably, despite these pronounced variations, our results reveal that the number of maxima per correlation length remains approximately constant across all fractality levels, as illustrated in the plots of Fig. 6.

This behavior can be understood from the spectral and wavefunction properties characteristic of electrons in fractal lattices. For a noninteracting electron gas with nearest-neighbor hopping, the coordination number remains bounded (with a maximum value of four), which constrains the energy spectrum to the interval $[-4t, 4t]$. However, the presence of fractal geometry strongly modifies the structure of the spectrum, leading to the emergence of quasidegenerate levels and highly irregular spectral distributions. In this regime, the corresponding eigenstates become critical and fractal, displaying strong spatial fluctuations rather than extending uniformly throughout the lattice. As a consequence, the effective correlation length of the wave functions can become comparable

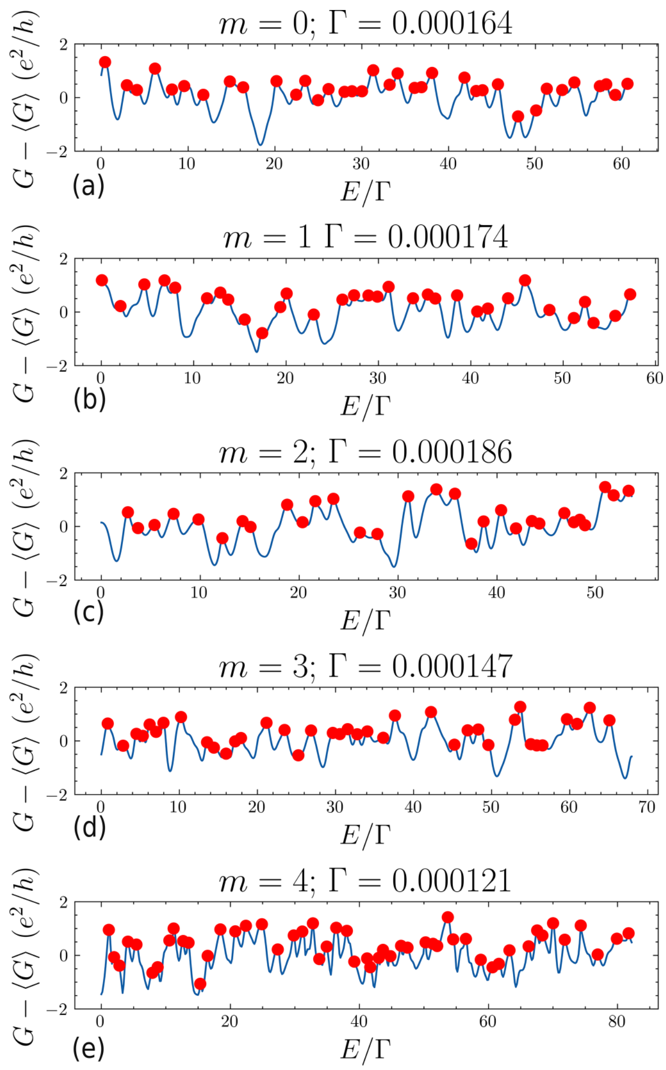

FIG. 6. (a)–(e) Density of local maxima of the conductance fluctuation signal, $G - \langle G \rangle$, as a function of the fractal iteration level.

to the system size. When the Fermi energy is tuned across the spectrum (for instance via a gate voltage), the conductance $G(E)$ exhibits sharp resonant variations whenever the energy approaches an eigenvalue of the system. The resulting sequence of peaks and valleys in the conductance traces is therefore a direct manifestation of quantum interference effects in the presence of critical states, providing a natural explanation for the increasing density of maxima observed as the fractal iteration level m grows. Similar spectral and transport features in fractal lattices have been discussed in recent studies [59,60].

The identification of local maxima in a energy-dependent signal $I(E)$, where $I \in \{G, P\}$ is a fundamental procedure in the characterization of complex systems, particularly those exhibiting multifractal behavior or governed by stochastic dynamics [20,21,61]. A point E is considered a local maximum if the following condition is satisfied over a small interval $[E, E + \delta E]$:

$$I'(E) > 0 \quad \text{and} \quad I'(E + \delta E) < 0, \tag{16}$$

where δE is sufficiently small. This condition ensures that $I(E)$ increases before E and decreases afterward, characterizing a local extremum.

Expanding $I'(E+\delta E)$ via a Taylor expansion around E yields the inequality

$$-I''(E)\delta E > I'(E) > 0, \tag{17}$$

where $I'(E)$ and $I''(E)$ denote the first and second energy derivatives of the signal, respectively. Here $I''(E)$ captures the local curvature, providing insight into the sharpness of the peak.

To statistically characterize the occurrence of such maxima, we introduce the joint probability distribution $P(I', I'')$, representing the likelihood of observing given values of I' and I''. Integrating over the admissible region defined by inequality (17), one obtains the expected density of maxima per unit time:

$$\int_{-\infty}^{0} dI'' \int_{0}^{-I''\delta E} dI' P(I', I'') = -\delta E \int_{-\infty}^{0} dI'' I'' P(0, I'') \equiv \delta E \langle\rho\rangle, \tag{18}$$

where $\langle\rho\rangle$ denotes the mean density of maxima. This expression formally connects the statistics of the signal's derivatives to the expected frequency of extrema.

Such an approach is particularly well suited to the analysis of signals with complex structures, where multiscale fluctuations result in nontrivial distributions of extrema. In the present context, this formalism allows for a quantitative assessment of how fractal spatial features influence temporal observables.

The joint distribution $P(I', I'')$ can be approximated using the lower-order moments of I' and I''. Since the signals under consideration are derived from statistically homogeneous energy series (i.e., invariant under translations in t), the mean values of both derivatives vanish. The second-order moments, however, are related to the autocorrelation function of the fluctuation signal $I^{\rm fl}(t) \equiv I(t) - \langle I(t)\rangle$, defined as

$$C(\delta E) \equiv \langle I^{\rm fl}(E + a\delta E) I^{\rm fl}(E - b\delta E)\rangle, \tag{19}$$

with the constraint $a + b = 1$. Differentiating $C(\delta E)$ with respect to δt yields:

$$\begin{aligned} \langle I'^2\rangle &= -\frac{d^2}{d(\delta E)^2} C(\delta E)\bigg|_{\delta t=0}, \\ \langle I' I''\rangle &= \frac{d^2}{d(\delta E)^2} C(\delta E)\bigg|_{\delta E=0}, \\ \langle I''^2\rangle &= \frac{d^4}{d(\delta E)^4} C(\delta E)\bigg|_{\delta E=0}, \end{aligned} \tag{20}$$

along with $\langle I I'\rangle = 0$ and $\langle I' I''\rangle = 0$ under stationarity and symmetry assumptions.

Assuming Gaussian statistics and employing the maximum entropy principle, the joint distribution $P(0, I'')$ takes the form

$$P(0, I'') = \frac{1}{2\pi} \frac{1}{\sqrt{\langle I'^2\rangle \langle I''^2\rangle}} \exp\left(-\frac{1}{2} \frac{I''^2}{\langle I''^2\rangle}\right). \tag{21}$$

Substituting this result into Eq. (18) and evaluating the integral, we arrive at the final expression:

$$\langle\rho\rangle = \frac{1}{2\pi} \sqrt{\frac{\langle I''^2\rangle}{\langle I'^2\rangle}}. \tag{22}$$

According to the central limit theorem, this result becomes increasingly accurate as the number of data points in the energy series grows. The use of the maximum entropy framework reflects the underlying assumption of "molecular chaos," which posits that the microscopic dynamics of the system introduce sufficient randomness such that correlations between $I(E)$ and $I(E+\delta E)$ are effectively captured through Gaussian statistics. This connection between signal derivatives and the density of extrema provides a robust foundation for linking spatial fractality to experimentally accessible temporal observables.

For each generated signal, we computed the autocorrelation function across all ensembles and fractal levels m. As an example, Fig. 7 shows the results for the ensemble $\beta = 1$, for both conductance and shot noise. A clear distinction is observed in the behavior of the autocorrelation curves for the different signals.

To quantify these curves, we fitted them using the following normalized generalized Lorentzian function

$$C(\delta\epsilon) = \frac{1}{[1 + (\delta\epsilon/\Gamma)^{2n}]^l}, \tag{23}$$

where Γ rescales the curves so that the correlation length is unity, and (l, n) are a fitting parameter. Equation (23) reduces to the standard Lorentzian profile when $(l, n) = (1, 1)$.

The parameters n and l in Eq. (23) control the shape of the generalized Lorentzian correlation function. While Γ defines the correlation length, the exponent n governs the curvature of the correlation peak at small energy separations, reflecting the short-range structure of the interference pattern. The parameter l, in turn, controls the weight of the long-energy tails of the correlation function and therefore quantifies the persistence of long-range correlations. In the absence of fractality, the universal prediction of random-matrix theory corresponds to the Lorentzian form $(n, l) = (1, 1)$. As the fractal iteration level increases, we observe a systematic increase of l accompanied by a monotonic decrease of n. This behavior indicates that the fractal geometry progressively suppresses long-range correlations while simultaneously introducing multiscale interference structures at short energy scales. These trends provide further evidence that scattering across the hierarchical lacunae of the fractal geometry fundamentally modifies the spectral correlations of quantum transport.

Figure 7 reveals a key result: for $m = 0$, the autocorrelation matches the Lorentzian profile accurately. However, as the fractal level m increases, the conductance curves progressively deviate from the Lorentzian form (indicated by the black line), suggesting that spatial fractality drives the system away from the Lorentzian form.

By substituting Eq. (23) into Eq. (18), we obtain the mean density of maxima in the correlation length scale Γ as

$$\langle\rho\rangle = \frac{\sqrt{6}}{2\pi} \sqrt{n(l+1)}. \tag{24}$$

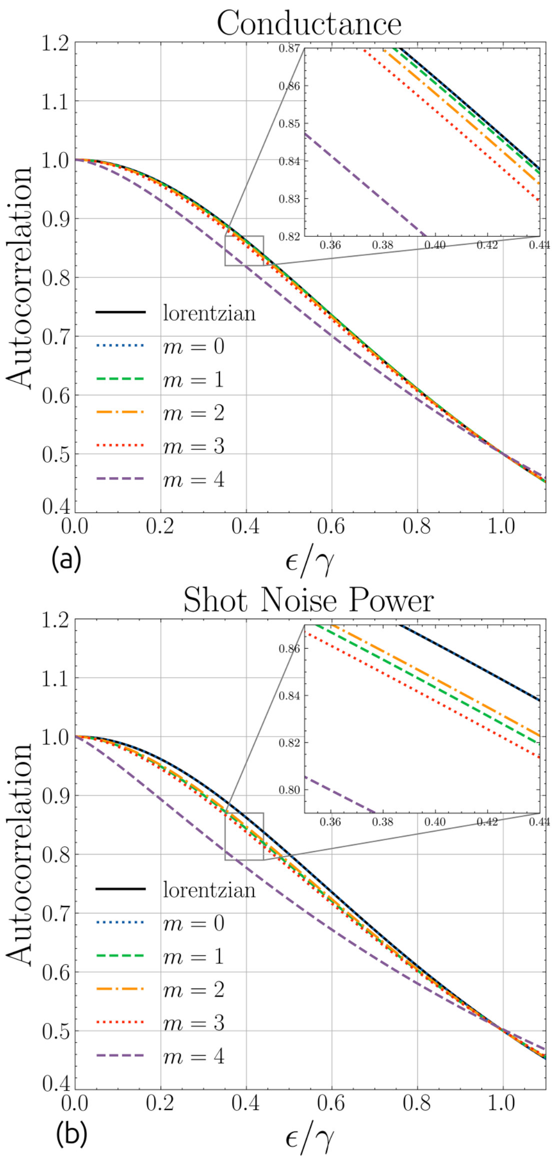

FIG. 7. (a) Autocorrelation functions fitted with the generalized Lorentzian for conductance. (b) Autocorrelation functions fitted with the generalized Lorentzian for shot noise power.

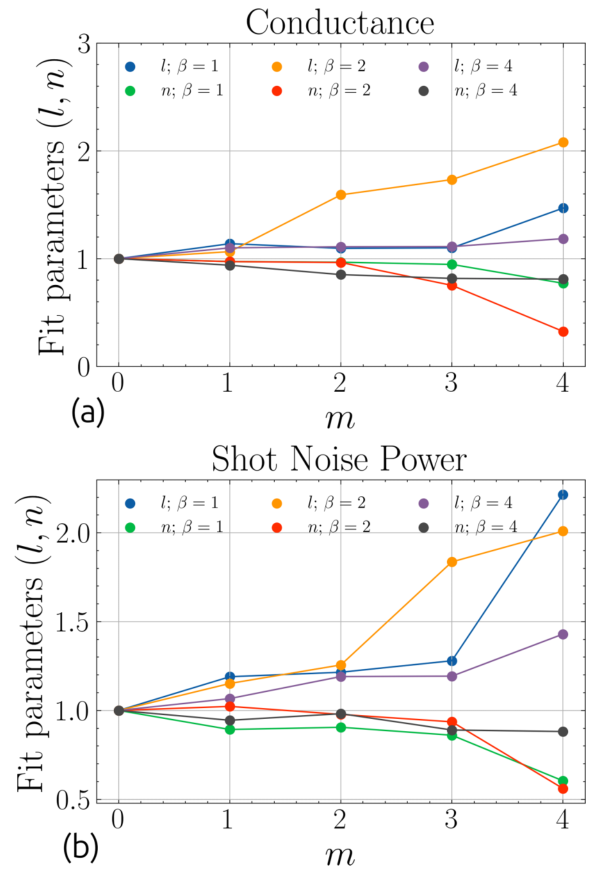

FIG. 8. Fitted values of the Lorentzian pair exponents (l, n) as functions of the fractal iteration level m, obtained for all Wigner-Dyson symmetry classes and for both observables for (a) conductance and (b) shot noise power.

The prediction given by Eq. (24) demonstrates that the correlation length can, in principle, be extracted from a single measurement of the observable by simply counting the density of local maxima N within a finite energy interval ΔE, since $\langle\rho\rangle = N/(\Delta E/\Gamma)$, which implies that

$$\Gamma = \frac{N}{\Delta E}\frac{1}{\langle\rho\rangle}. \tag{25}$$

This result further indicates that the density of maxima is a function of the pair (l, n), which in turn depends on the fractality index m. In Fig. 8 we present the extracted values of (l, n) for all three Wigner-Dyson ensembles as functions of the fractal iteration level. One observes that the parameter l increases systematically with the fractal iteration level m, starting from the Lorentzian case ($l = 1$). This behavior indicates that increasing fractal complexity drives the system away from the standard Lorentzian or square-Lorentzian functional forms, progressively weakening the correlations in the transport signal. Conversely, the parameter n decreases monotonically with increasing m. In the asymptotic limit $m \to \infty$, the correlation length is expected to vanish, indicating a transition to an uncorrelated regime.

This analysis was repeated for all three symmetry classes ($\beta = 1, 2, 4$), and for both conductance and shot noise signals, over all fractal depths m. In all cases the density of maxima increased consistently with m.

Figure 8 summarizes the evolution of the fitted (l, n) parameters across all symmetry classes and for both types of observables: conductance and shot noise power. Generalizing the trend previously discussed for conductance, the parameter l increases substantially and monotonically with the fractal iteration level m, remaining close to unity at $m = 0$, i.e., in the absence of fractality, for both observables. This behavior confirms that fractality not only enhances the complexity of the measured signals, but also induces systematic and quantifiable deviations from the correlation statistics expected in nonfractal, homogeneous systems.

Finally, we note that the density of local maxima—and, consequently, the correlation length—can be extracted via Eqs. (20), (22), (23), following the fitting of the empirical correlation function using Eq. (23). It is important to emphasize that this fitting procedure requires a statistically significant number of independent realizations of the conductance and

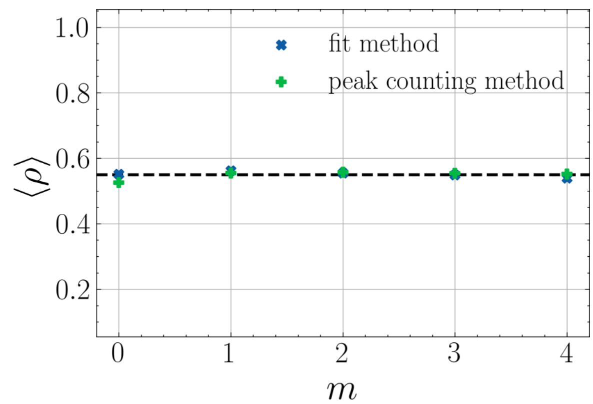

FIG. 9. Number of maxima per correlation length ρ versus the fractal iteration m. Despite the opposite trends of the fitted exponents (l, n), ρ converges to the universal value $\rho \approx \sqrt{3}/\pi \approx 0.55$ for conductance.

shot noise power traces. The resulting estimates, obtained through this ensemble-averaged approach, are shown in blue in Fig. 9 as a function of the fractal iteration index m.

A major advantage of the framework we propose lies in the fact that the same quantity—the density of maxima—can also be estimated from a single empirical realization of the signal. The corresponding results are displayed in green in Fig. 9, showing excellent agreement with the ensemble-based estimates. This agreement supports both the applicability of the maximum entropy principle and the robustness of chaos statistics in fractal quantum dots.

Interestingly, the number of maxima within one correlation length is found to decrease with increasing m, as shown in Fig. 9. This trend highlights an anomalous effect of fractality when compared to known universal behaviors in chaotic quantum dots. In contrast, when considering fixed energy intervals (rather than fixed correlation lengths), we observe the opposite effect: the number of maxima increases by approximately one order of magnitude as m increases, as illustrated in Fig. 4. This again reflects a significant reduction of the correlation length with increasing fractal complexity.

Remarkably, despite these contrasting trends, the number of maxima per correlation length converges to the universal value $\rho \approx 0.55$ $(\sqrt{3}/\pi)$ for the conductance signal. This behavior indicates that the competing contributions of the parameters (l, n) in the generalized correlation function mutually compensate each other: as fractal complexity increases, one parameter enhances correlations while the other suppresses them, leading to an overall universal outcome, as Fig. 9 indicates.

VI. CONCLUSION

In this work we have elucidated the fundamental role of fractal geometry in modulating the universal features of quantum transport in mesoscopic systems. Our analysis of Sierpiński carpet structures has revealed that the fractal dimension of conductance and shot noise fluctuations increases systematically with the fractal iteration level. Crucially, we have demonstrated that this geometric complexity directly governs the fractality of the transport curves, with the fractal dimension of the underlying structure correlating robustly with that of the observable fluctuations. This correspondence holds across all symmetry classes—GOE, GUE, and GSE—indicating that electron scattering through the internal voids of the fractal geometry is the dominant mechanism shaping transport in the universal regime. Accordingly, the shot-noise power $P(E)$ is analyzed as an independent and complementary observable, confirming that the emergence of fractal scaling is not restricted to conductance fluctuations but represents a robust feature of quantum transport in fractal geometries. This behavior is consistent with the interpretation that the observed fluctuations originate from interference and resonant transport across multiple scattering paths, while the analysis of shot noise provides an independent verification that the same geometric complexity governs different transport observables.

Furthermore, we have shown that, although the density of local maxima in the conductance traces increases with fractality and the correlation length decreases accordingly, the number of maxima per correlation length remains remarkably. This invariance, together with the observed deviation of the autocorrelation function from the Lorentzian profile as fractality increases, highlights the extent to which non-Euclidean geometry imprints a distinct signature on quantum transport. In particular, the evolution of the generalized correlation parameters suggests that increasing fractal complexity leads to a progressive suppression of long-range correlations.

Taken together, these findings not only deepen our understanding of transport in complex quantum systems, but also open promising avenues for the geometric engineering of materials and devices. The ability to design the fluctuation spectrum and correlation length of quantum transport via geometric manipulation of the scattering region introduces a new paradigm for controlling electronic properties at the nanoscale. Future investigations may explore the asymptotic behavior of the fluctuation fractal dimension, and examine whether similar geometric-spectral correspondences arise in other classes of fractal structures. These directions may ultimately consolidate geometry-based design as a key principle in the emerging landscape of quantum electronic engineering.

DATA AVAILABILITY

There are no publicly available research data or software supporting this manuscript. Requests for further information or data should be sent to the authors.

[1] F. Haake, *Quantum Signatures of Chaos*, 3rd ed. (Springer, Berlin, 2010).

[2] H.-J. Stöckmann, *Quantum Chaos: An Introduction* (Cambridge University Press, Cambridge, 1999).

[3] T. Guhr, A. Müller-Groeling, and H. A. Weidenmüller, Random-matrix theories in quantum physics: Common concepts, Phys. Rep. **299**, 189 (1998).

[4] N. Bohr, Neutron capture and nuclear constitution, Nature (London) **137**, 344 (1936).

[5] C. Mahaux and H. A. Weidenmüller, *Shell-Model Approach to Nuclear Reactions* (North-Holland, Amsterdam, 1969).

[6] E. P. Wigner, On the statistical distribution of the widths and spacings of nuclear resonance levels, Proc. Cambridge Philos. Soc. **47**, 790 (1951).

[7] G. E. Mitchell, A. Richter, and H. A. Weidenmüller, Random matrices and chaos in nuclear physics: Nuclear reactions, Rev. Mod. Phys. **82**, 2845 (2010).

[8] A. M. M. Argüello, M. Carrera-Núñez, and J. A. Méndez-Bermúdez, Scattering and transport properties of the three classical Wigner–Dyson ensembles at the Anderson transition, Phys. Rev. E **107**, 024139 (2023).

[9] A. K. Das and A. Ghosh, Nonergodic extended states in the β ensemble, Phys. Rev. E **105**, 054121 (2022).

[10] G. Cipolloni, L. Erdős, and D. Schröder, On the spectral form factor for random matrices, Commun. Math. Phys. **401**, 1665 (2023).

[11] M. Hopjan and L. Vidmar, Scale-invariant critical dynamics at eigenstate transitions, Phys. Rev. Lett. **131**, 060404 (2023).

[12] C. W. J. Beenakker, Random-matrix theory of quantum transport, Rev. Mod. Phys. **69**, 731 (1997).

[13] Y. Alhassid, The statistical theory of quantum dots, Rev. Mod. Phys. **72**, 895 (2000).

[14] T. Heinzel, *Mesoscopic Electronics in Solid State Nanostructures* (Wiley-VCH, Weinheim, 2003).

[15] K. Kawabata, Z. Xiao, T. Ohtsuki, and R. Shindou, Singular-value statistics of non-Hermitian random matrices and open quantum systems, PRX Quantum **4**, 040312 (2023).

[16] A. M. García-García, L. Sá, and J. J. M. Verbaarschot, Universality and its limits in non-Hermitian many-body quantum chaos using the Sachdev–Ye–Kitaev model, Phys. Rev. D **107**, 066007 (2023).

[17] F. Roccati, F. Balducci, R. Shir, and A. Chenu, Diagnosing non-Hermitian many-body localization and quantum chaos via singular value decomposition, Phys. Rev. B **109**, L140201 (2024).

[18] R. Duda, M. N. Ivaki, I. Sahlberg, K. Pöyhönen, and T. Ojanen, Quantum walks on random lattices: Diffusion, localization, and the absence of parametric quantum speedup, Phys. Rev. Res. **5**, 023150 (2023).

[19] P. A. Lee, A. D. Stone, and H. Fukuyama, Universal conductance fluctuations in metals: Effects of finite temperature, interactions, and magnetic field, Phys. Rev. B **35**, 1039 (1987).

[20] J. G. G. S. Ramos, D. Bazeia, M. S. Hussein, and C. H. Lewenkopf, Conductance peaks in open quantum dots, Phys. Rev. Lett. **107**, 176807 (2011).

[21] L. G. C. S. Sá, A. L. R. Barbosa, and J. G. G. S. Ramos, Conductance peak density in disordered graphene topological insulators, Phys. Rev. B **102**, 115105 (2020).

[22] M. L. Mehta, *Random Matrices*, 3rd ed. (Elsevier, Amsterdam, 2004).

[23] R. Landauer, Spatial variation of currents and fields due to localized scatterers in metallic conduction, IBM J. Res. Dev. **1**, 223 (1957).

[24] M. Büttiker, Four-terminal phase-coherent conductance, Phys. Rev. Lett. **57**, 1761 (1986).

[25] R. Blümel and U. Smilansky, Classical irregular scattering and its quantum-mechanical implications, Phys. Rev. Lett. **60**, 477 (1988).

[26] R. A. Jalabert, H. U. Baranger, and A. D. Stone, Conductance fluctuations in the ballistic regime: A probe of quantum chaos? Phys. Rev. Lett. **65**, 2442 (1990).

[27] K. B. Efetov, Temperature effects in quantum dots in the regime of chaotic dynamics, Phys. Rev. Lett. **74**, 2299 (1995).

[28] B. B. Mandelbrot, *The Fractal Geometry of Nature* (W. H. Freeman, New York, 1982).

[29] K. J. Falconer, *Fractal Geometry: Mathematical Foundations and Applications*, 3rd ed. (John Wiley & Sons, Chichester, 2014).

[30] S. H. Strogatz, *Nonlinear Dynamics and Chaos: With Applications to Physics, Biology, Chemistry, and Engineering,* 2nd ed. (Westview Press, Boulder, 2015).

[31] S. N. Kempkes, M. R. Slot, S. E. Freeney, S. J. M. Zevenhuizen, D. Vanmaekelbergh, I. Swart, and C. M. Smith, Design and characterization of electrons in a fractal geometry, Nat. Phys. **15**, 127 (2019).

[32] L. Lage and A. Latgé, Electronic fractal patterns in building Sierpinski-triangles molecular systems, Phys. Chem. Chem. Phys. **24**, 19576 (2022).

[33] B. Pal and K. Saha, Flat bands in fractal-like geometry, Phys. Rev. B **97**, 195101 (2018).

[34] D. Leykam, A. Andreanov, and S. Flach, Artificial flat band systems: From lattice models to experiments, Adv. Phys. X. **3**, 1473052 (2018).

[35] X. Zhang, G. Gu, N. Li, H. Wang, H. Tang, Y. Zhang, S. Hou, and Y. Wang, One-dimensional molecular chains formed by Sierpiński triangles on Au(111), RSC Adv. **8**, 1852 (2018).

[36] F. L. Sendker, Y. K. Lo, T. Heimerl, S. Bohn, L. J. Persson, C.-N. Mais, W. Sadowska, N. Paczia, E. Nußbaum, M. C. Sánchez Olmos, K. Forchhammer, D. Schindler, T. J. Erb, J. L. P. Benesch, E. G. Marklund, G. Bange, J. M. Schuller, and G. K. A. Hochberg, Emergence of fractal geometries in the evolution of a metabolic enzyme, Nature (London) **628**, 894 (2024).

[37] A. Gowrisankar and S. Banerjee, Frontiers of fractals for complex systems: Recent advances and future challenges, Eur. Phys. J.: Spec. Top. **230**, 3743 (2021).

[38] J. Dai, X. Zhao, Z. Peng, J. Li, Y. Lin, X. Wen, L. Xing, W. Zhao, J. Shang, Y. Wang, J. Liu, and K. Wu, Assembling surface molecular Sierpiński triangle fractals via K^+-invoked electrostatic interaction, J. Am. Chem. Soc. **145**, 13531, (2023).

[39] H. Hennig, R. Fleischmann, L. Hufnagel, and T. Geisel, Fractal conductance fluctuations of classical origin, Phys. Rev. E **76**, 015202(R) (2007).

[40] X.-Y. Xu, X.-W. Wang, D.-Y. Chen, C. M. Smith, and X.-M. Jin, Quantum transport in fractal networks, Nat. Photon. **15**, 703 (2021).

[41] E. van Veen, S. Yuan, M. I. Katsnelson, M. Polini, and A. Tomadin, Quantum transport in Sierpinski carpets, Phys. Rev. B **93**, 115428 (2016).

[42] A. K. Slimane, P. Reck, and G. Fleury, Simulating time-dependent thermoelectric transport in quantum systems, Phys. Rev. B **101**, 235413 (2020).

[43] M. M. Odashima and C. H. Lewenkopf, Time-dependent resonant tunneling transport: Keldysh and Kadanoff–Baym nonequilibrium Green's functions in an analytically soluble problem, Phys. Rev. B **95**, 104301 (2017).

[44] Z. Yu, L. Zhang, Y. Xing, and J. Wang, Investigation of transient heat current from first principles using complex absorbing potential, Phys. Rev. B **90**, 115428 (2014).

[45] M. Ridley, M. Galperin, E. Gull, and G. Cohen, Numerically exact full counting statistics of the energy current in the Kondo regime, Phys. Rev. B **100**, 165127 (2019).

[46] Y. V. Nazarov and Y. M. Blanter, *Quantum Transport: Introduction to Nanoscience* (Cambridge University Press, Cambridge, 2009).

[47] C. W. Groth, M. Wimmer, A. R. Akhmerov, and X. Waintal, KWANT: A software package for quantum transport, New J. Phys. **16**, 063065 (2014).

[48] Ya M. Blanter and M. Büttiker, Shot noise in mesoscopic conductors, Phys. Rep. **336**, 1 (2000).

[49] M. Büttiker, Scattering theory of current and intensity noise correlations in conductors and wave guides, Phys. Rev. B **46**, 12485 (1992).

[50] Th Martin and R. Landauer, Wave-packet approach to noise in multichannel mesoscopic systems, Phys. Rev. B **45**, 1742 (1992).

[51] Y. V. Nazarov and M. Kindermann, Full counting statistics of a general quantum mechanical variable, Eur. Phys. J. B **35**, 413 (2003).

[52] M. Büttiker, Quantized transmission of a saddle-point constriction, Phys. Rev. B **41**, 7906 (1990).

[53] E. van Veen, A. Tomadin, M. Polini, M. I. Katsnelson, and S. Yuan, Optical conductivity of a quantum electron gas in a Sierpinski carpet, Phys. Rev. B **96**, 235438 (2017).

[54] X. Yang, W. Zhou, Q. Yao, P. Lv, Y. Wang, and S. Yuan, Electronic properties and quantum transport in functionalized graphene Sierpinski-carpet fractals, Phys. Rev. B **105**, 205433 (2022).

[55] Y. Wang, W. Zhou, Q. Yao, P. Lv, and S. Yuan, Electronic states and quantum transport in bilayer graphene Sierpinski-carpet fractals, Phys. Rev. B **109**, 235429 (2024).

[56] P. A. Lee and A. D. Stone, Universal conductance fluctuations in metals, Phys. Rev. Lett. **55**, 1622 (1985).

[57] T. Kiss and I. Jex, Photons walk on fractal graphs, Nat. Photon. **15**, 641 (2021).

[58] A. Rojo-Francàs, P. Pansari, U. Bhattacharya, B. Juliá-Díaz, and T. Grass, Anomalous quantum transport in fractal lattices, Commun. Phys. **7**, 259 (2024).

[59] Q. Yao, X. Yang, A. A. Iliasov, M. I. Katsnelson, and S. Yuan, Energy-level statistics in planar fractal tight-binding models, Phys. Rev. B **107**, 115424 (2023).

[60] Q. Yao, X. Yang, A. A. Iliasov, M. I. Katsnelson, and S. Yuan, Wave functions in the critical phase: A planar Sierpiński fractal lattice, Phys. Rev. B **110**, 035403 (2024).

[61] D. Bazeia, M. B. P. N. Pereira, A. V. Brito, B. F. de Oliveira, and J. G. G. S. Ramos, A novel procedure for the identification of chaos in complex biological systems, Sci. Rep. **7**, 44900 (2017).